Large As sublattice distortion in sphalerite ZnSnAs2 thin films revealed by x-ray fluorescence holography

Kouichi Hayashi, Naotaka Uchitomi, Keitaro Yamagami, Akiko Suzuki, Hayato Yoshizawa, Joel T. Asubar, Naohisa Happo, and Shinya Hosokawa

Articles you may be interested in

Epitaxial Cu2ZnSnS4 thin film on Si (111) 4° substrate
Appl. Phys. Lett. **106**, 252102 (2015); 10.1063/1.4922992

Inhomogeneous distribution of manganese atoms in ferromagnetic ZnSnAs2:Mn thin films on InP revealed by three-dimensional atom probe investigation
J. Appl. Phys. **117**, 17B905 (2015); 10.1063/1.4914065

Investigation of combinatorial coevaporated thin film Cu2ZnSnS4. I. Temperature effect, crystalline phases, morphology, and photoluminescence
J. Appl. Phys. **115**, 173502 (2014); 10.1063/1.4871664

Magnetization dependence on electron density in epitaxial ZnO thin films codoped with Mn and Sn
J. Appl. Phys. **97**, 053904 (2005); 10.1063/1.1856225

Studies of Mn/GaAs digital alloys using x-ray absorption fine structure and x-ray diffraction methods
Appl. Phys. Lett. **80**, 2654 (2002); 10.1063/1.1467982

Large As sublattice distortion in sphalerite ZnSnAs$_2$ thin films revealed by x-ray fluorescence holography

Kouichi Hayashi,[1,a] Naotaka Uchitomi,[2] Keitaro Yamagami,[2] Akiko Suzuki,[2] Hayato Yoshizawa,[2] Joel T. Asubar,[3] Naohisa Happo,[4] and Shinya Hosokawa[5]

[1]*Department of Materials Science and Engineering, Nagoya Institute of Technology, Nagoya 466-8555, Japan*
[2]*Department of Electrical Engineering, Nagaoka University of Technology, Nagaoka 940-2188, Japan*
[3]*Graduate School of Engineering, University of Fukui, Fukui 910-8507, Japan*
[4]*Graduate School of Information Sciences, Hiroshima City University, Hiroshima 731-3194, Japan*
[5]*Department of Physics, Graduate School of Science and Technology, Kumamoto University, Kumamoto 860-8555, Japan*

The structure of a ZnSnAs$_2$ thin film epitaxially grown on an InP substrate was evaluated using x-ray fluorescence holography. The reconstructed three-dimensional atomic images clearly show that the crystal structure of the ZnSnAs$_2$ thin film is mainly of the sphalerite type, in contrast to the bulk form. A large disordering of the As layers is observed, whereas the positions of the Zn/Sn atoms are relatively stable. The analysis of the data indicates that the As layers serve as a buffer and relax the strain caused by the random occupation of Zn and Sn atoms. These results provide further understanding and a means of controlling the growth of Mn-doped ZnSnAs$_2$, a high-T_c diluted magnetic semiconductor. © *2016 AIP Publishing LLC.*
[http://dx.doi.org/10.1063/1.4945004]

I. INTRODUCTION

Over the last five years, x-ray fluorescence holography[1] (XFH) has been used for various types of structural characterization of crystals, such as to clarify the local environments and lattice distortions around impurity atoms,[2,3] the formation of local-[4] and intermediate-range[5,6] clusters, and lattice distortions around specific elements.[7,8] These results are not easy to obtain by conventional diffraction or x-ray absorption fine structure (XAFS) experiments. Another difficulty in the structural characterization of crystals addressed in this article is the quantitative determination of crystal forms in disordered systems.[9]

For example, the solar cell material ZnSnP$_2$ has a chalcopyrite structure in the bulk form at room temperature.[10] Bulk ZnSnP$_2$ is known to undergo an order–disorder (chalcopyrite-sphalerite) transition at 720 °C.[11] With the change in crystal symmetry, the electronic structure varies and the band gap significantly decreases from 1.66 to 1.24 eV upon the transition.[12] The band gaps of chalcopyrite and sphalerite ZnSnP$_2$ thin films were also reported to be 1.683 and 1.383 eV, respectively.[13] The coexistence of equilibrium ordered- and nonequilibrium disorder phases has been discussed for epitaxial ZnSnP$_2$ films on GaAs substrates using high-resolution x-ray diffraction (XRD). This coexistence depends on Zn/Sn flux ratio[14] and the substrate temperature during growth.[15] Thus, this material in the thin-film form can have a mixture of chalcopyrite and sphalerite phases with different band gaps but the same chemical composition.

In principle, a specific structure in thin films can be precisely detected by high-resolution XRD measurements by observing specific Bragg peaks characteristic of the structure, as was carried out by Francoeur *et al*. for ZnSnP$_2$ thin films.[15] They also determined Bragg-William order parameter characterized by the average long-range order in the mixed sublattice. For analyzing the order degree of the chalcopyrite structure, infrared or Raman spectra of ZnSnP$_2$ thin films are useful by referring to the structural model given in Ref. 14. Moreover, further investigation of structural processes, such as the lattice distortions and cluster formations around specific elements, is difficult to perform by only using these conventional methods.

In this study, we investigated ZnSnAs$_2$ thin film epitaxially grown on an InP substrate.[16] II-IV-V$_2$ ternary compound semiconductors are known as promising materials for thermophotovoltaic solar cells, nonlinear optics, and infrared detectors.[17,18] There has been renewed interest in ZnSnAs$_2$ after a report of room-temperature ferromagnetism in Mn-doped bulk ZnSnAs$_2$.[19] Such ferromagnetism has also been investigated in thin film grown on InP substrate by molecular beam epitaxy (MBE).[20,21]

In bulk form under ambient conditions, ZnSnAs$_2$ crystallizes in the stable chalcopyrite structure (space group: I$\bar{4}$2d) with $a = 5.851$ and $c = 11.702$ Å, which undergoes a transformation at 655 °C (Ref. 22) to the metastable sphalerite structure (space group: F$\bar{4}$3m) with the same a value.[10] In the chalcopyrite structure (see the insets of Figs. 2(b) and 2(c), Zn and Sn atoms are tetrahedrally coordinated with four As atoms, and the As atoms are tetrahedrally bonded with two Zn and two Sn atoms in a specific order. Two identical *fcc* cells are stacked on each other to form a body-centered tetragonal structure, which may produce optical anisotropy. In the sphalerite structure (see the inset of Fig. 2(d)), on the other hand, Zn and Sn atoms are randomly distributed on the cation sublattice, and there is no optical

a)Author to whom correspondence should be addressed. Electronic mail: khayashi@nitech.ac.jp.

anisotropy, although the local structure is similar to that of the chalcopyrite structure.

Similar to the $ZnSnP_2$ crystal, different optical and electronic properties are expected in the $ZnSnAs_2$ crystal for the chalcopyrite and sphalerite structures owing to the structural ordering in the chalcopyrite form. To our knowledge, however, there had been no measurements to verify this. Nevertheless, it is very important for applications to quantitatively know the fraction of chalcopyrite and sphalerite structures in thin films of this alloy crystal.

XFH provides three-dimensional (3D) atomic images around a specific element emitting its own fluorescent x-rays.[1] Recent technical advances in XFH using intense synchrotron radiation facilities have enabled 3D images to be reproduced with a diameter of a 10 Å order, called *middle-range local structures*. Moreover, XFH is very sensitive to positional fluctuations of each of neighboring atoms. Note that the As atoms in $ZnSnAs_2$ are much more clearly visible in XFH than the P atoms in $ZnSnP_2$ because the x-ray scattering ability of As is much greater than that of P.

In this paper, we report the results of Zn $K\alpha$ XFH experiments on a $ZnSnAs_2$ thin film epitaxially grown on an InP substrate. From the reconstructed 3D atomic image, we not only quantitatively determine the crystal type but also clarify the sublattice distortions in the thin film. On the basis of these structural results, we discuss its structural features as a host material for the room-temperature ferromagnetic semiconductor Mn-doped $ZnSnAs_2$.

II. EXPERIMENTAL PROCEDURE

A $ZnSnAs_2$ epitaxial single-crystal layer was grown on a semi-insulating InP substrate with a (001) surface by MBE using a procedure described elsewhere.[20,21] The homogeneity of the thin film was monitored by reflection high-energy electron diffraction during the growth of the film. The film thickness was chosen to be 500 nm. The structure of the sample film was examined using XRD, and it was confirmed that the sample was of high single-crystal quality. Bragg peaks characteristic of the chalcopyrite structure was not clearly identified from the XRD data. A GaAs thin film with the same thickness was also grown on a Ge(001) substrate by MBE as a reference in the XFH measurement. Then, the samples were cut to a surface size of $10 \times 10\,mm^2$.

The XFH experiment was carried out at the beamline BL6C of the Photon Factory in the High Energy Accelerator Research Organization (PF-KEK) in Tsukuba, Japan. The Zn $K\alpha$ fluorescent x-rays were collected using an avalanche photodiode detector with a cylindrical graphite energy analyzer. The measurements were performed by rotating two axes of the sample, $0° \leq \theta \leq 75°$ in steps of $1.0°$ and $0° \leq \phi \leq 360°$ in steps of $\sim 0.35°$, and detecting the small modulations with angles of about 0.3%. Such holograms were recorded with 15 different energies of the incident x-rays of 9.3–13.8 keV in steps of 0.25 keV. The average count rate of the Zn $K\alpha$ fluorescent x-rays was about 200 000 cps, and each scan took about 3 h. One of the aims of the present work was quantitative determination of atomic fluctuations like our past studies.[2,8] To perform this, we needed a

standard sample, in which mean square displacements of atoms were already determined by other method. To avoid the sample form effect, we chose a GaAs thin film, not a GaAs bulk. Therefore, we measured Ga $K\alpha$ holograms of this sample under the same experimental condition.

Holographic oscillation data were obtained by subtracting the background from the fluorescent x-ray intensities and normalizing them by the incident x-ray intensities. The statistical improvement of the holographic data was carried out by twofold-symmetrizing the raw data using the crystallographic symmetry of the chalcopyrite and sphalerite crystal structures and the measured x-ray standing wave (XSW) lines.

For comparison with the experimental data, a theoretical hologram was obtained using chalcopyrite and sphalerite crystal model clusters by simulating the scattering in the crystals. The lattice constants of the chalcopyrite and sphalerite forms were fixed to the values obtained by XRD by Vaipolin *et al.*,[10] and the cluster radius was about 60 Å with about 33 500 atoms around the central Zn atom. Atomic scattering intensities from neighboring atoms were simulated using atomic form factors,[23] Debye-Waller factors,[24] and absorption coefficients[25] obtained from the literature. The calculations were performed using our own codes based on those in the literature.[26,27]

III. RESULTS

Figure 1 shows the Zn $K\alpha$ hologram measured at an incident x-ray energy of 9.8 keV. The sharp lines observed in the pattern are the XSW lines, which indicate the high crystallinity of the $ZnSnAs_2$ film. From the fifteen Zn $K\alpha$ holograms with different incident x-ray energies, we reconstructed real-space images around Zn using Barton's multiple-energy holography algorithm.[28]

Figure 2(a) shows the resultant atomic images on the (001) plane at $z = 0.0$ Å. All the atomic images displayed here are of the cation atoms of Zn and Sn. The atomic images at all the sites in this plane can be clearly observed, and the intensity appears to monotonically decrease with increasing distance from the center.
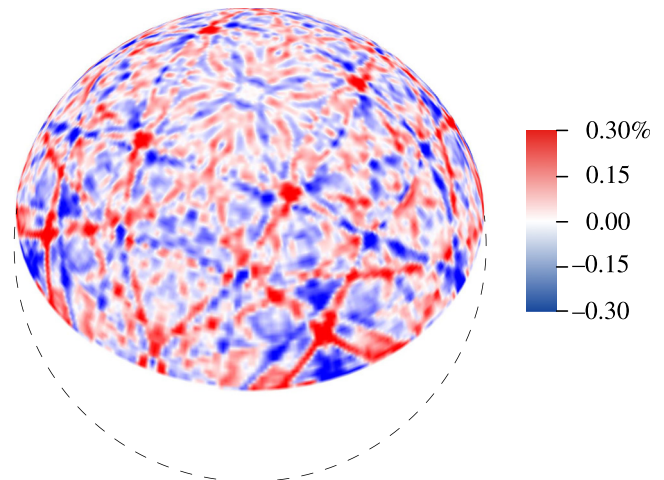

FIG. 1. X-ray fluorescence hologram of $ZnSnAs_2$ thin film measured at 9.8 keV.
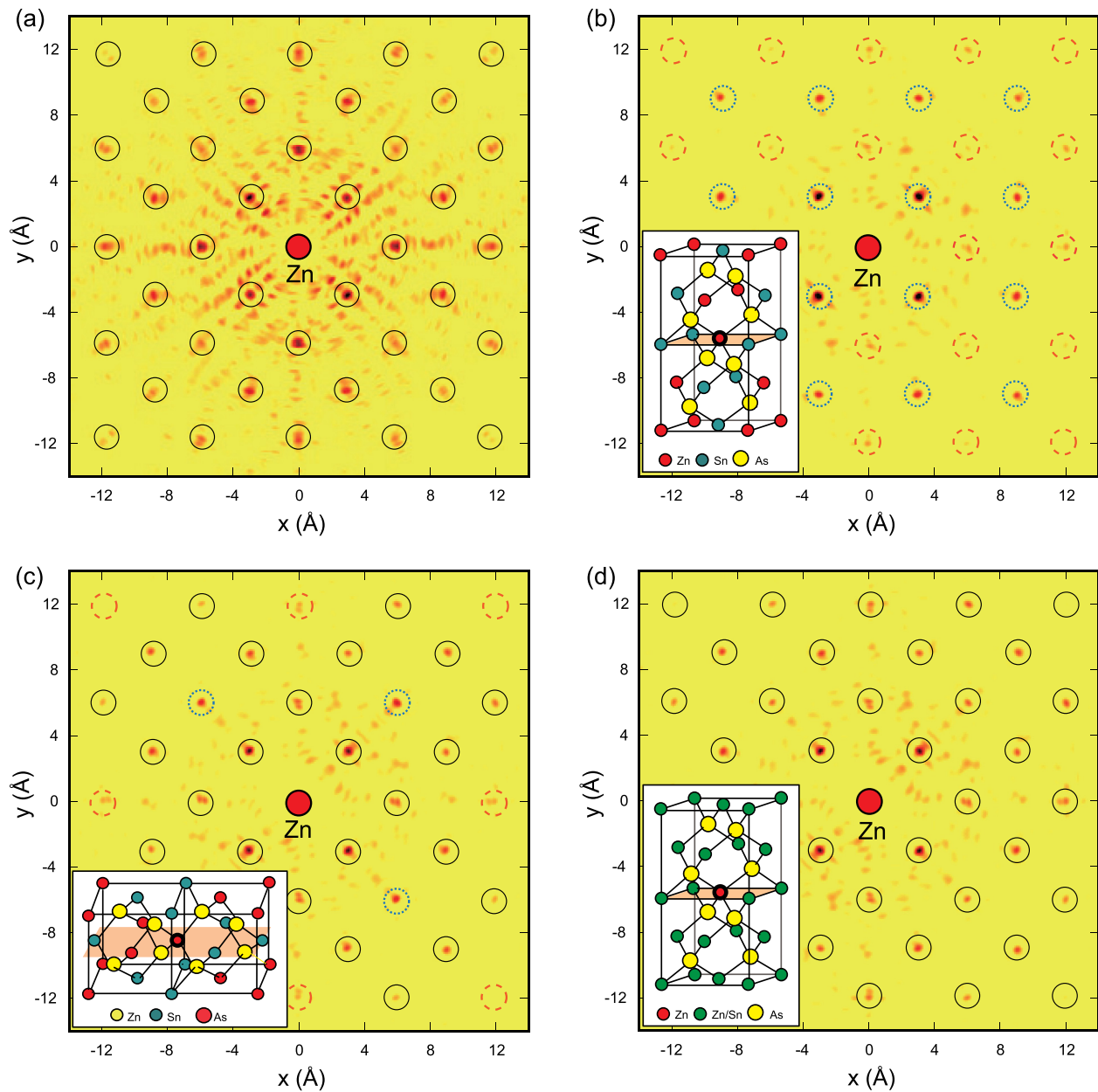
FIG. 2. Atomic images on the (001) plane at $z = 0.0$ Å around the central Zn atom obtained from (a) experimental holograms and theoretical holograms using the models of (b) *c*-axis- and (c) *a*-axis-oriented chalcopyrite, and (d) sphalerite structures. The insets are the structure models used for the hologram calculations. The solid circles in (a) indicate ideal cation positions. The dotted and dashed circles in (b) and (c) indicate the positions of Sn and Zn atoms, respectively. The solid circles in (c) and (d) indicate the overlapping positions of Zn and Sn atoms.

ZnSnAs$_2$ film films fabricated by MBE had believed to form chalcopyrite structure. To determine the major structure of the ZnSnAs$_2$ film, we calculated holograms using the structure models of chalcopyrite and sphalerite. Differently from XRD, long range-periodicity is not necessary for XFH. XFH can analyze locally ordered chalcopyrite structure, as well. To check out any possibilities of chalcopyrite structure, we modeled *c*-axis and *a*-axis models for the hologram calculations, as shown in the insets in Figs. 2(b) and 2(c). In addition to these, holograms of the sphalerite structure model were calculated as a last possibility. Figure 2(b) shows the atomic image on the (001) plane at $z = 0.0$ Å reconstructed from theoretical holograms of the *c*-axis-oriented chalcopyrite structure. The atomic arrangement of this model is displayed in the inset. Note that for this theoretical image,

we considered four different orientations of the clusters with the *c*-axis parallel to the [100], [$\bar{1}$00], [010], and [0$\bar{1}$0] directions of the InP substrate, but the atoms on this plane are *identical* in these clusters. As can be clearly seen in the figure, the atomic images indicated by the dotted circles are much stronger than those shown by the dashed circles, because the former and latter images correspond to the Sn and Zn atoms, respectively, and the x-ray scattering cross section of Sn is much larger than that of Zn.

Figure 2(c) shows the atomic image on the (001) plane at $z = 0.0$ Å reconstructed from theoretical holograms of the *a*-axis-oriented chalcopyrite structure model. As mentioned above, there are four different orientations of the *a*-axis in the chalcopyrite model cluster. The image is reconstructed from the average of the holograms of four *different* clusters

with the *c*-axis parallel to the [100], [$\bar{1}$00], [010], and [0$\bar{1}$0] directions. In contrast to Fig. 2(b), the atomic images indicated by solid circles thus correspond to the averaged images of the Sn and Zn atoms.

Figure 2(d) shows the atomic images on the (001) plane at $z = 0.0$ Å obtained from the sphalerite structure model. All the atomic images of the sphalerite structure model are attributed to the average of Sn and Zn images. The differences between Figs. 2(c) and 2(d) appear only for the distant atoms, where the compositions of the cation elements are different. In the *a*-oriented chalcopyrite model in Fig. 2(c), the second atoms in the diagonal directions at a length of 8.275 Å are always Sn atoms, and the second atoms in the horizontal and vertical directions at 11.702 Å are always the Zn atoms, while those in the sphalerite structure model are always the averaged values of the Sn and Zn atoms.

IV. DISCUSSION

A. Structural determination of ZnSnAs$_2$ thin film

To determine the structure of the ZnSnAs$_2$ thin film, we plot in Fig. 3 the intensities of the experimental images (solid lines) and calculated images (dashed lines) from the (a) *c*- and (b) *a*-oriented chalcopyrite structure models and (c) the sphalerite structure model as a function of the distance from the central Zn atom.
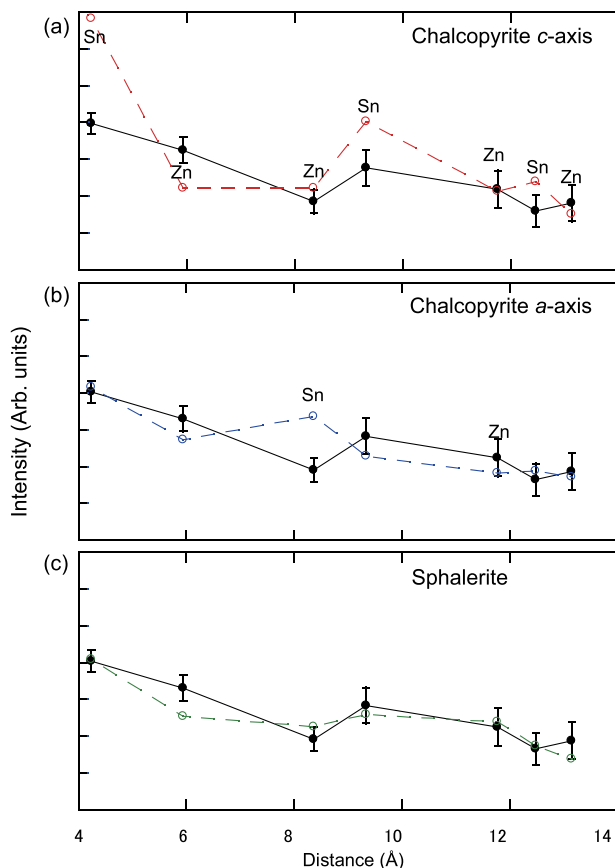
In Fig. 3(a), large discrepancies can be observed between the image intensities in the experiment and the *c*-oriented chalcopyrite model at every neighboring atom, as mentioned above for the comparison between Figs. 2(a) and 2(b). In the *c*-oriented chalcopyrite model, the first- (4.137 Å), fourth- (9.251 Å), and sixth- (12.412 Å) neighboring atoms on this plane are composed of only Sn atoms having a larger x-ray scattering cross section than Zn atoms, where the theoretical values considerably exceed the experimental data. On the other hand, the second- (5.851 Å), third- (8.275 Å), fifth- (11.702 Å), and seventh- (13.083 Å) neighboring atoms on this plane are composed of only Zn atoms, where the theoretical image intensities are slightly lower or similar to the experimental values. Thus, the *c*-oriented chalcopyrite model is not a suitable structure for the present ZnSnAs$_2$ thin film.

In Fig. 3(b), the coincidence between the image intensities in the experiment and the *a*-oriented chalcopyrite model is much improved. However, a positive discrepancy is realized at the third-neighboring atomic images on this plane, which are solely composed of the Sn atoms in the *a*-oriented chalcopyrite model clusters.

The result for the sphalerite model cluster is shown in Fig. 3(c), where the coincidence between the experimental and theoretical image intensities is excellent. Compared with the calculated intensity variations using the two chalcopyrite structure models, the result using the sphalerite crystal structure model is more similar to the experimental result. Therefore, we can conclude that the dominant structure in the ZnSnAs$_2$ thin-film sample is of the sphalerite type, and that the crystal structure of ZnSnAs$_2$ in the thin-film form is different from that in the bulk form.[19]

Since there appear to be small differences between the sphalerite and *a*-oriented chalcopyrite models, it would be useful to examine the fraction of the chalcopyrite structures in the ZnSnAs$_2$ thin film in detail. Figure 4 shows the sum of the squared residuals of the model intensities obtained with the *c*- (full circles) and *a*-oriented (empty circles)

FIG. 3. Intensities of the atomic images as a function of the distance from the center in (a) *c*-axis-oriented chalcopyrite, (b) *a*-axis-oriented chalcopyrite, and (c) sphalerite structures. Solid and dashed lines indicate the experimental and calculated data, respectively.
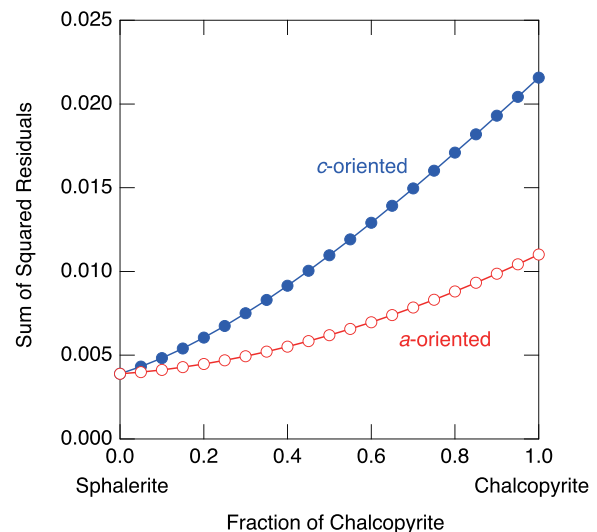
FIG. 4. Sum of squared residuals between the experimental and model image intensities as a function of the chalcopyrite fraction. The results for the *c*- and *a*-oriented chalcopyrite models are given by full and empty circles, respectively.

chalcopyrite models with respect to the experimental image intensities as a function of the fraction of the chalcopyrite structure. Note that the calculations were performed in steps of 5% and that the errors are within the size of the marks. As can be clearly seen in the figure, the sum of the squared residuals monotonically decreases with decreasing fraction of either the *c*- or *a*-oriented chalcopyrite structures. It is thus concluded that the crystal structure of the $ZnSnAs_2$ thin film is mainly of the sphalerite type within an error of 5%.

B. Positional fluctuations of As atoms in sphalerite structure

Since the sample mostly has the sphalerite structure, we can extend the hologram from a limited θ range to the 4π full angle range using the fourfold rotational and mirror symmetries of the sphalerite crystal structure. An example of the fully symmetrized result at an incident x-ray energy of 9.8 keV is given in Fig. 5.

The obtained 4π holograms greatly improve the spatial resolution of the images, making it possible to more quantitatively discuss the atomic images. Figures 6(a)–6(c) show reconstructed images at $z = 0.0$, 1.46, and 2.92 Å, respectively. All the images at $z = 0.0$ Å in Fig. 6(a) correspond to the average of the Zn and Sn cation images, which are clearly observed up to the edges of the figure. In contrast, the images of As at $z = 1.46$ Å in Fig. 6(b) are very weak except for the As image at (3/4, 1/4, 1/4) and its equivalents. The cation images at $z = 2.92$ Å in Fig. 6(c) are again clearly visible.

The intensity of an atomic image is basically proportional to the atomic number and inversely proportional to the distance from the origin. Since the atomic number of As (33) is 82.5% of the average of the atomic numbers of Zn (30) and Sn (50), the atomic number does not cause a significant decrease in the As image intensity. In addition to the above factors, the image intensity decreases with the positional fluctuations of atoms.[2] Therefore, it can be inferred that the main reason for the decrease in the As image intensity should be the large positional fluctuations of the As atom sites with
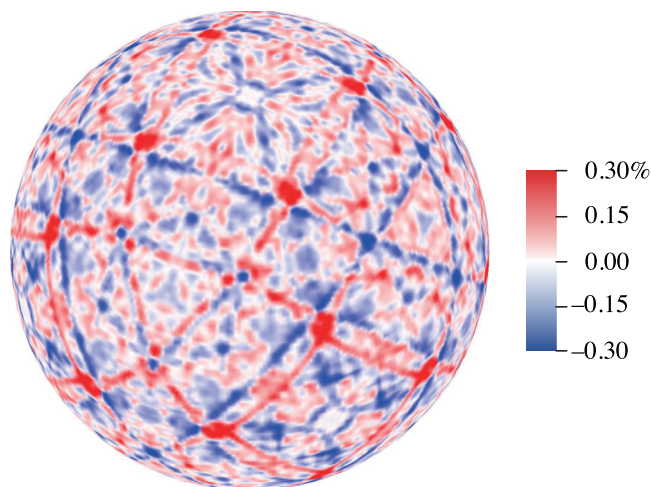

FIG. 5. Fully symmetrized x-ray fluorescence hologram of $ZnSnAs_2$ thin film measured at 9.8 keV.

respect to the central Zn atom. If this is the case, it is surprising that the As atoms are more positionally disordered than the cations even though the cation sites are randomly occupied by Zn or Sn atoms.

To quantitatively analyze the extent of the fluctuations of the As and Zn/Sn in the $ZnSnAs_2$ film, we fabricated a GaAs thin film ($\sim$500 nm) on a Ge substrate as a reference sample and measured the Ga $K\alpha$ holograms. Principally, a mean square displacement of atom is determined by the intensity reduction due to the fluctuation of atom. This reduction rate is indirectly obtained by comparing with a standard sample whose mean square displacements of the atoms were already estimated by other methods, as discussed below. Figures 6(d)–6(f) show the atomic images at $z = 0.0$, 1.41, and 2.82 Å, respectively. The images of Ga atoms appear at $z = 0.0$ and 2.82 Å, and those of As atoms appear at 1.41 Å. Since Ge substrate does not have cation and anion layers, during epitaxial growth both the Ga and As layers do not stack selectively on two kinds of crystallographic Ge layers, unlike the case of $ZnSnAs_2$/InP. Therefore, the As images of the GaAs film exhibit two zinc-blende-type atomic arrangements with different orientations. We assumed that the occupancy of the As atom at each site is random, and thus we doubled the As image intensities in Fig. 6(e) to enable a fair comparison. In Figs. 6(d)–6(f), the As images are clearly visible as well as the Ga images, in contrast to the As images in the $ZnSnAs_2$ film shown in Fig. 6(b). This result confirms the higher degree of positional disorder of the As atoms in the $ZnSnAs_2$ film.

Using the reconstructed atomic images of the $ZnSnAs_2$ and reference GaAs thin films shown in Fig. 6, the image intensities are plotted as a function of the distance from the central Zn or Ga atom in Fig. 7. All the intensities are normalized to the atomic numbers of the elements of the neighboring atoms and then to the highest intensity of the first-neighboring As images of GaAs. These data were fitted by the simple formula a_1/d, where d is the distance from the central Zn or Ga atom and a_1 is a fitting parameter, giving the positional stabilities of the atoms. Since some correlations are observed for near-neighboring atoms, particularly for the As images at (3/4, 1/4, 1/4), the fitting was carried out in the distance range of 5–16 Å.

The obtained a_1 values for Ga (GaAs), As (GaAs), Zn/Sn ($ZnSnAs_2$), and As ($ZnSnAs_2$) are 2.52, 2.92, 1.58, and 1.09, respectively. From these values, we estimated the atomic positional fluctuation, i.e., the mean square displacement of the neighboring scatterer atom relative to the central emitter atom, σ. The σ dependence of the image intensity was calculated using the multiple-energy hologram of a simple dimer model,[8] and the results are given in Fig. 8.

The σ values of Ga and As in GaAs were reported to be 0.089 and 0.078 Å, respectively.[29] In XFH, the atomic fluctuations are regarded as the relative displacements from the central atom emitting fluorescent x-rays. Thus, the two values of σ for the emitting and scatterer atoms should be convoluted to discuss the image intensities. The convoluted value for the Ga pair, σ_{Ga-Ga}, is 0.125 Å and that for Ga and As, σ_{Ga-As}, is 0.117 Å. These values are plotted in Fig. 8, and the intensities of 0.73 and 0.70 were obtained for σ_{Ga-Ga} and σ_{Ga-As}, respectively. These intensity values correspond
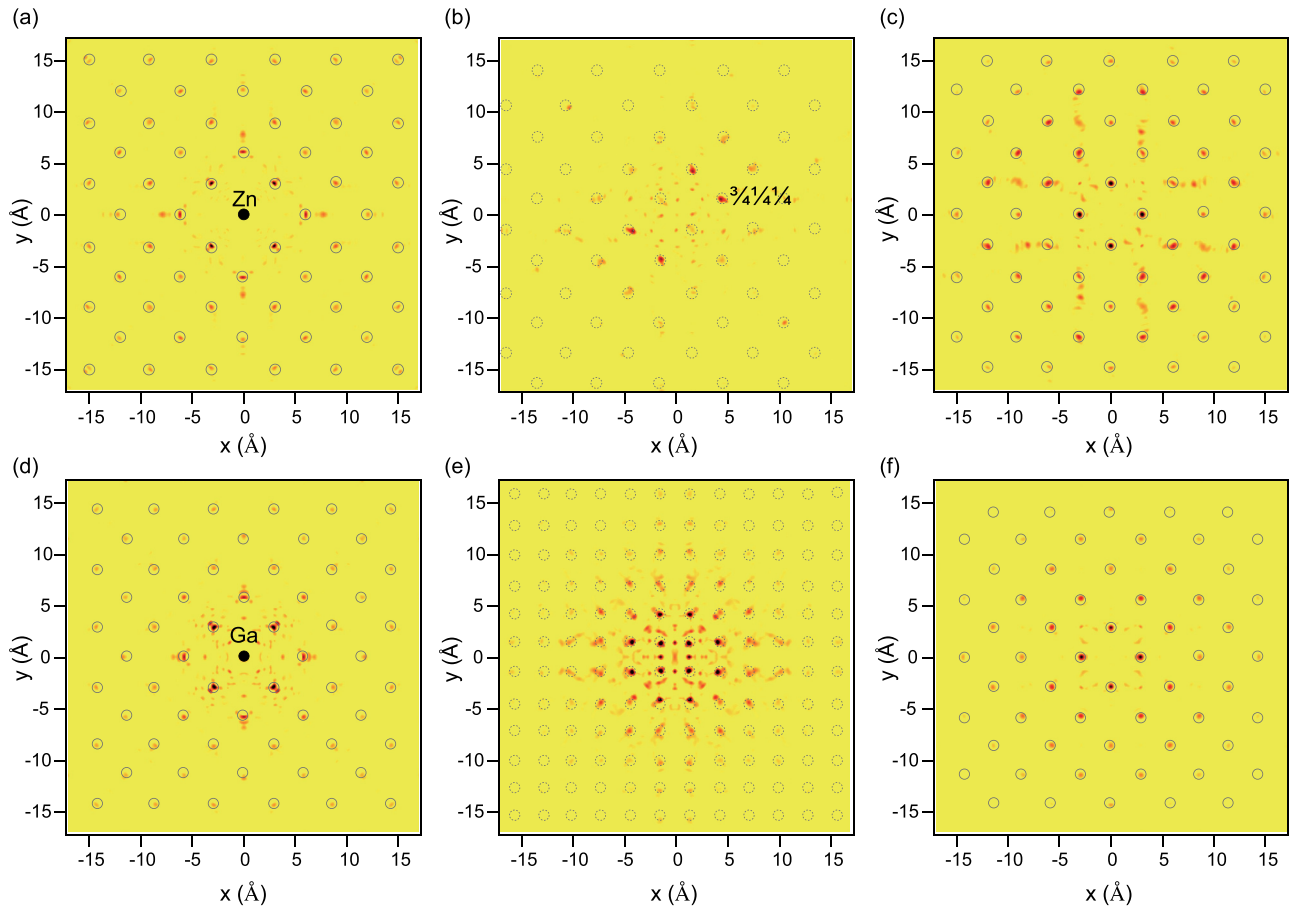
FIG. 6. Atomic images on the (001) planes around Zn or Ga obtained from the 4π holograms. The images in (a)–(c) are of the $ZnSnAs_2$ film and those in (d)–(f) are of the reference GaAs film. (a) $z = 0.0$ Å, (b) $z = 1.46$ Å, (c) $z = 2.92$ Å, (d) $z = 0.0$ Å, (e) $z = 1.41$ Å, and (f) $z = 2.82$ Å. The intensities of the As images in (e) are doubled. The circles in each images indicate ideal positions of atoms.

to $a_1 = 2.52$ and 2.92 for Ga and As in GaAs, respectively. Thus, it is clarified that the larger a_1 value for the As images originates from the smaller fluctuation of As atoms in GaAs.

To quantitatively estimate the atomic fluctuations in the $ZnSnAs_2$ thin film, we define the average of σ_{Ga-Ga} and σ_{Ga-As}, 0.121 Å for GaAs, as the standard σ value. This σ value corresponds to a normalized intensity of 0.715, the average of 0.73 for Ga-Ga and 0.70 for Ga-As, as indicated by the dashed line in Fig. 8. The averaged a_1 value (2.72) of
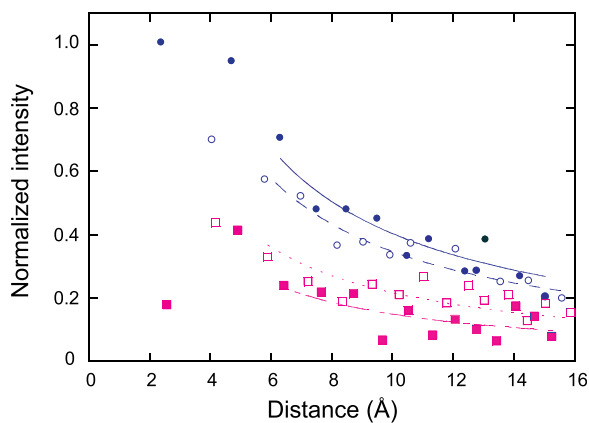

FIG. 7. Intensities of the atomic images as a function of the distance from the origin. The open and filled squares indicate the intensities of Zn/Sn and As images in $ZnSnAs_2$, respectively. The dotted and dotted-dashed lines indicate the fitting curves for the Zn/Sn and As images, respectively. The open and filled circles indicate the intensities of the Ga and As images in GaAs, respectively. The dashed and solid lines indicate the fitting curves for the Ga and As images, respectively. All intensities are normalized to the atomic numbers of the elements.
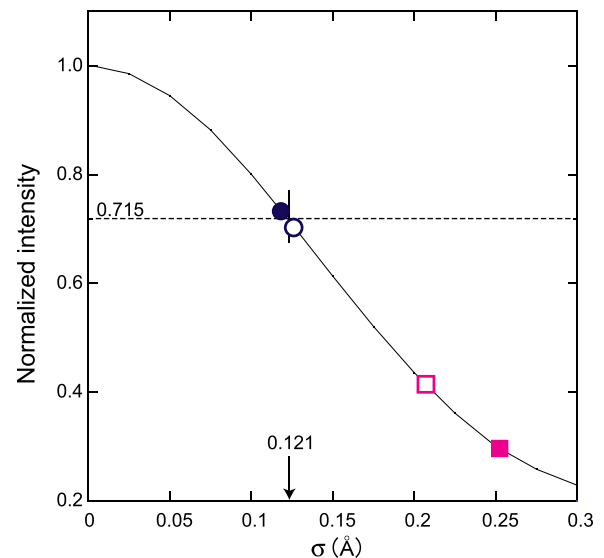

FIG. 8. σ dependence of image intensity on the atomic fluctuation. The intensity is normalized to its highest value at $\sigma = 0$ Å. Open and filled circles indicate the Ga and As image intensities in GaAs, respectively. Open and filled squares indicate the (Zn, Sn) and As image intensities in $ZnSnAs_2$, respectively.

Ga-Ga (2.52) and Ga-As (2.92) corresponds to the normalized image intensity of 0.715 on the line in Fig. 8.

By calculating the ratios of the a_1 values for the ZnSnAs$_2$ crystal to the reference value of 2.72 for GaAs, we can quantitatively obtain the fluctuations of Zn/Sn and As. The ratios of $a_1 = 1.58$ for Zn/Sn and 1.09 for As in ZnSnAs$_2$ to the averaged value of 2.72 for GaAs are 0.58 and 0.40, respectively. By taking the reduction factor of 0.72 into account, the normalized intensities are calculated to be 0.41 for Zn/Sn and 0.29 for As around the central Zn atom. From Fig. 8, the σ values are consequently estimated to be 0.207 Å for $\sigma_{Zn-Zn/Sn}$ and 0.255 Å for σ_{Zn-As}.

These σ values are much larger than the reference value of $\sigma_{Ga-Ga/As} = 0.121$ Å for GaAs. This can be easily understood from the large value of $\sigma_{Zn-Zn/Sn} = 0.207$ Å because the Zn and Sn atoms occupy the same atomic sites with different atomic radii similar to mixed crystals such as In$_{1-x}$Ga$_x$Sb (Ref. 2) and Zn$_{1-x}$Mn$_x$Te (Ref. 8) for which large positional fluctuations have been observed in the mixed sites by XFH. However, it is interesting that a much larger σ_{Zn-As} value is observed for the Zn-As correlation even though the anion sites are occupied by only a single As element.

To evaluate σ values for the neighboring Zn/Sn and As, it is expedient to assume that the σ value for the central Zn atom in ZnSnAs$_2$ equals that for the central Ga atom in GaAs of 0.089 Å. Balzarotti *et al.* and Jeong *et al.* also treated the atomic fluctuations of different cations as same in their analyses of zinc-blend type mixed crystals.[31,32] Using this assumption, $\sigma_{Zn/Sn} = 0.146$ Å and $\sigma_{As} = 0.209$ Å are obtained by the deconvolutions of $\sigma_{Zn-Zn/Sn}$ and σ_{Zn-As}, respectively. The σ_{As} value of an anion site is 43% larger than the $\sigma_{Zn/Sn}$ value of a cation site with a mixture of Zn and Sn.

C. Comparison with existing models

To understand the structural features obtained by the present XFH experiment and the analysis of the ZnSnAs$_2$ thin film, it is useful to compare the results with the existing structural models for mixed crystals. Balzarotti *et al.* measured the XAFS on mixed crystals of the diluted magnetic semiconductor Cd$_{1-x}$Mn$_x$Te having a zinc-blende crystal structure and obtained the bimodal distribution of the nearest-neighbor distances of Cd-Te and Mn-Te.[30,31] To reconcile this XAFS result with diffraction data exhibiting Vegard's rule of proportional changes in nearest-neighbor distance with the cation ratio, they proposed a model named Balzarotti's model in which the anion atoms are displaced from the ideal crystallographic positions by a large number, whereas the cation sublattice remains undistorted even in a mixture of Cd and Mn atoms with different atomic radii. This model appears to be reasonable for the present ZnSnAs$_2$ thin film.

Jeong *et al.* measured the high-energy XD on the semiconductor In$_x$Ga$_{1-x}$As and obtained atomic pair distribution functions (PDFs) with a high real-space resolution and the bimodal distribution of the nearest-neighbor distances.[32] Combining this structural information with a theoretical

calculation using the Kirkwood potential, they evaluated the local atomic displacements and found that the value of σ for the static disorder of the cation sublattice is 60% smaller than that for the static disorder of the anion sublattice. Therefore, Balzarotti's structural model of atomic spatial fluctuations appears to match our present XFH results for the ZnSnAs$_2$ thin film.

We previously proposed a different model to explain the XFH result for a mixed crystal of Zn$_{0.4}$Mn$_{0.6}$Te.[8] This model is the so-called locomotive wheel model, where the average positions of the atoms coincide with the corresponding lattice positions obtained by the XD experiment, while the actual atoms are located on spheres with certain diameters centered at the lattice positions to agree with the XAFS data. In the case of Zn$_{0.4}$Mn$_{0.6}$Te, the diameters of the cation and anion are the same in the model, i.e., the positional fluctuations are the same for the cation and anion. The model perfectly reproduces the XD and XAFS data as shown in Fig. 8 of Ref. 8 and would explain the atomic image intensities obtained from the XFH measurement.

In the ZnSnAs$_2$ thin film, on the other hand, the positional fluctuations in the As sublattice are more prominent than those in the Zn/Sn cation sublattice, although larger fluctuations are expected in the cation sublattice owing to the different atomic sizes of the Zn and Sn atoms. Thus, it can be concluded that the diameters of the spheres should be reconsidered for the locomotive wheel model to adopt it as a structural model for the ZnSnAs$_2$ thin film.

D. Features and roles of distorted As sublattice

Finally, we discuss the correlations between the central Zn and neighboring As atoms. Figures 9(a) and 9(b), respectively, show the real-space images of the As layers at $z = 1.46$ and 4.38 Å. In these planes, strong As images can be seen as indicated by arrows. These images appear within a radius of 7 Å. However, the first-neighboring and distant (beyond 7 Å) As images are very weak. The former observation has been reported for several mixed crystals, while the latter observation is unusual.[2,8]

To discuss this unique feature, the number of chemical bonds between the central Zn and neighboring As atoms is counted. The solid and dashed arrows in Figs. 9(a) and 9(b) indicate the surrounding As atoms with three and five chemical bonds from the central Zn atom, respectively. As can be clearly seen in the figures, the strong atomic images correspond to the As atoms with three and five chemical bonds from the central Zn atom, regardless of the interatomic length. Thus, it is concluded that the positional fluctuations of the As atoms are not randomly spread over the ZnSnAs$_2$ crystal, and that some structural ordering exists with respect to the Zn atoms.

This structural feature of the As layer suggests that the As layer plays an important role as a buffer to self-optimize the structure of this mixed crystal. Namely, the positional disordering in the As layer is expected to be important for maintaining the crystal structure, because the As layer relaxes the strain caused by the random occupation of Zn and Sn atoms with different atomic sizes.
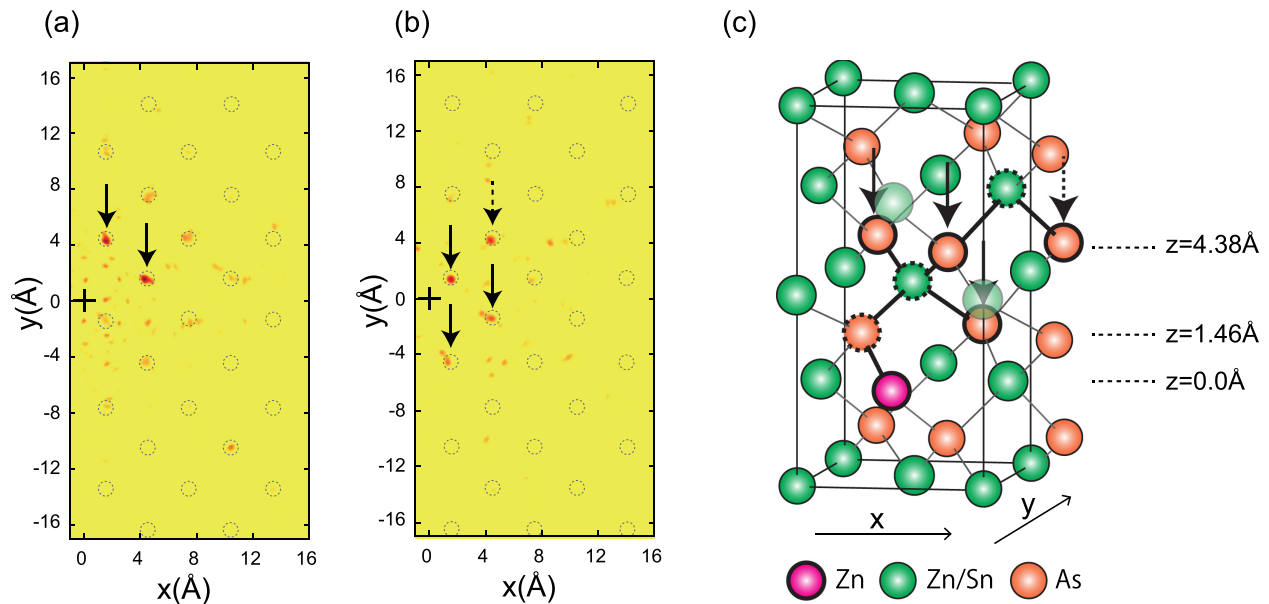
FIG. 9. Strong correlations between Zn and As. (a) and (b) show the images of As layers at $z = 1.46$ and 4.38 Å, respectively, and (c) sphalerite structure of ZnSnAs$_2$. Solid and dashed arrows indicate strongly correlated As atoms with three and five chemical bonds from the central Zn atom, respectively.

Considering the ZnSnAs$_2$ thin film as a host material for magnetic doping, the buffer-like layers should play a very important role in achieving a Mn doping level as high as 10%.[33] In the case of GaMnAs, the ferromagnetic nature appears upon the substitution of Mn impurities for Ga atoms. The Curie temperature T_C increases with the Mn concentration, reaches a maximum of 110 K approximately 6% Mn concentration, and then decreases with the further increase of Mn concentration.[34]

Recent experimental investigations of these ferromagnetic semiconductors have revealed that the T_C value was enhanced to 191 K after the postgrowth annealing of GaMnAs with nominally 20% Mn concentration, which was attributed to the out-diffusion of magnetically inactive interstitial Mn impurities toward the free epilayer surface during annealing.[35] On the other hand, detailed theoretical and experimental studies[36] have revealed that although the T_C can be increased up to 173 K,[37] only 6.8% of the Mn atoms can be substituted for Ga sites. Subsequently, doped Mn atoms preferentially occupy interstitial sites, which limit the attainable T_C value. The rigid configuration of the host GaAs lattice may introduce large lattice distortions around Mn atoms having different bond lengths with As, resulting in the loss of the asymmetry of local configurations and the eventual displacement of impurity atoms from substitutional sites. In the case of Cd$_{1-x}$Mn$_x$Te, Balzarotti *et al.* reported that when the addition of Mn into CdTe increases the ionicity of the bond, the local distributions of the tetrahedral stabilize the zinc-blend type structure up to $x = 0.7$ on the basis of their model.[31]

On the other hand, the As sites in the ZnSnAs$_2$ thin film are highly flexible in terms of their positions, as found in the present XFH study. Compared with GaAs, ZnSnAs$_2$ is expected to accommodate a higher Mn doping level while maintaining an undistorted MnAs$_4$ tetrahedral symmetry in the sphalerite structure.[38] Moreover, the random distribution

of the Zn/Sn cations in the sphalerite form may be stabilized by the fluctuation of the As sublattice layers inside the cubic structure, in contrast to the ordered chalcopyrite form, which is stable under thermal equilibrium.

Under such conditions, the buffer-like As layers in the sphalerite ZnSnAs$_2$ thin film may allow a higher magnetic Mn doping level and suppress the formation of magnetic secondary phases such as a NiAs-type hexagonal structure with sixfold coordination around the Mn atoms. Although this explanation requires further investigation in the future, we believe that the sphalerite ZnSnAs$_2$ thin film is highly advantageous for synthesizing ferromagnetic semiconductors with high T_C above room temperature.

In the present study, we have determined the fundamental structural information of a ZnSnAs$_2$ thin film. As our next task, we will carry out an XFH experiment on a Mn-doped ZnSnAs$_2$ thin film. We expect to obtain valuable knowledge on its relatively high Curie temperature by studying the local structure around Mn, particularly the correlations between Mn and other constituent elements.

V. CONCLUSIONS

We applied XFH to characterize the crystal structure and lattice distortions in a ZnSnAs$_2$ thin film. The analysis of atomic images revealed that the measured ZnSnAs$_2$ thin film mostly has a sphalerite structure and exhibits significantly larger positional disordering in the As layers than in the cationic layers, even though the Zn and Sn atoms randomly occupy the cation sites in the sphalerite structure. This structural feature of the As layers allows it to act as a buffer to self-optimize this mixed crystal. Namely, the As layers are important for maintaining the crystal structure because they relax the strains caused by the random occupation of the Zn and Sn atoms. This newly revealed structural feature may be very useful for understanding the lattice distortions when additional Mn dopants are added to a ZnSnAs$_2$ thin film to

induce a ferromagnetic nature at room temperature, at which the ferromagnetic properties are very sensitive to the local coordinations around the magnetic atoms.

ACKNOWLEDGMENTS

[1]K. Hayashi, N. Happo, S. Hosokawa, W. Hu, and T. Matsushita, J. Phys.: Condens. Matter **24**, 093201 (2012).

[2]S. Hosokawa, N. Happo, T. Ozaki, H. Ikemoto, T. Shishido, and K. Hayashi, Phys. Rev. B **87**, 094104 (2013).

[3]A pioneering work on Ge impurities in Si was described in K. Hayashi, Y. Takahashi, I. Yonenaga, and E. Matsubara, Mater. Trans. **45**, 1994 (2004).

[4]S. Hosokawa, N. Happo, S. Senba, T. Ozaki, T. Matsushita, A. Koura, F. Shimojo, and K. Hayashi, J. Phys. Soc. Jpn. **83**, 124602 (2014).

[5]W. Hu, K. Hayashi, T. Yamamoto, N. Happo, S. Hosokawa, T. Terai, T. Fukuda, T. Kakeshita, H. Xie, T. Xiao, and M. Suzuki, Phys. Rev. B **80**, 060202(R) (2009).

[6]W. Hu, K. Hayashi, T. Fukumura, K. Akagi, M. Tsukada, N. Happo, S. Hosokawa, K. Ohwada, M. Takahasi, M. Suzuki, and M. Kawasaki, Appl. Phys. Lett. **106**, 222403 (2015).

[7]N. Happo, K. Hayashi, S. Senba, H. Sato, M. Suzuki, and S. Hosokawa, J. Phys. Soc. Jpn. **83**, 113601 (2014).

[8]S. Hosokawa, N. Happo, and K. Hayashi, Phys. Rev. B **80**, 134123 (2009).

[9]W. Hu, K. Hayashi, K. Ohwada, J. Chen, N. Happo, S. Hosokawa, M. Takahasi, A. A. Bokov, and Z.-G. Ye, Phys. Rev. B **89**, 140103(R) (2014).

[10]A. S. Borshchevskii, A. A. Vaipolin, N. A. Goryunova, and G. V. Loshakova, Inorg. Mater. **4**, 772 (1968).

[11]N. A. Goryunova, I. I. Kozhina, G. V. Loshakova, and A. S. Borshchevskii, Vestn. Leningr. Univ., Ser. 4: Fiz., Khim. **22**, 159 (1967).

[12]M. A. Ryan, M. W. Peterson, D. L. Williamson, J. S. Frey, G. E. Maciel, and B. A. Parkinson, J. Mater. Res. **2**, 528 (1987).

[13]P. St-Jean, G. A. Seryogin, and S. Francoeur, Appl. Phys. Lett. **96**, 231913 (2010).

[14]G. A. Seryogin, S. A. Nikishin, H. Temkin, A. M. Mintairov, J. L. Merz, and M. Holtz, Appl. Phys. Lett. **74**, 2128 (1999).

[15]S. Francoeur, G. A. Seryogin, S. A. Nikishin, and H. Temkin, Appl. Phys. Lett. **74**, 3678 (1999).

[16]G. A. Seryogin, S. A. Nikishin, H. Temkin, R. Schlaf, L. I. Sharp, Y. C. Wen, B. Parkinson, V. A. Elyukhin, Yu. A. Kudriavtsev, A. M. Mintairov, N. N. Faleev, and M. V. Baidakova, J. Vac. Sci. Technol., B **16**, 1456 (1998).

[17]J. L. Shay and J. H. Wernick, *Ternary Chalcopyrite Semiconductors: Growth, Electronic Properties and Application* (Pergamon Press, New York, 1975).

[18]V. O. G. Folberth and H. Pfister, Acta Crystallogr. **13**, 199 (1960).

[19]S. Choi, G.-B. Cha, S. C. Hong, S. Cho, Y. Kim, J. B. Ketterson, S.-Y. Jeong, and G.-C. Yi, Solid State Commun. **122**, 165 (2002).

[20]J. T. Asubar, A. Kato, T. Kambayashi, Y. Jinbo, and N. Uchitomi, J. Cryst. Growth **301–302**, 656 (2007).

[21]J. T. Asubar, Y. Jinbo, and N. Uchitomi, J. Cryst. Growth **311**, 929 (2009).

[22]E. Yu Tonkov, *High Pressure Phase Transformations Handbook 1* (Gordon and Breach Science Publishers, Philadelphia, 1992), p. 71.

[23]*International Tables for Crystallography*, edited by A. J. C. Wilson and V. Geist (Kluwer, Dordrecht, 1992), Vol. C.

[24]C. Kittel, *Introduction to Solid State Physics*, 7th ed. (Wiley, New York, 1996), p. 126.

[25]S. Sasaki, KEK Report No. 90-16, National Laboratory for High Energy Physics, Tsukuba, 1991, p. 1.

[26]P. M. Len, S. Thevuthasan, C. S. Fadley, A. P. Kaduwela, and M. A. Van Hove, Phys. Rev. B **50**, 11275 (1994).

[27]P. M. Len, Ph.D. thesis, University of California-Davis, June 1997, see http://www.icts.hkbu.edu.hk/surfstrucinfo/SurfStrucInfo_files/holo/holopack.html.

[28]J. J. Barton, Phys. Rev. Lett. **67**, 3106 (1991).

[29]A. W. Stevenson, Acta Crystallogr., Sect. A: Found. Adv. **50**, 621 (1994).

[30]A. Balzarotti, M. Czyżnyk, A. Kisiel, N. Motta, M. Podgòrny, and M. Zimnal-Starnawska, Phys. Rev. B **30**, 2295 (1984).

[31]A. Balzarotti, N. Motta, A. Kisiel, M. Zimnal-Starnawska, M. T. Czyżnyk, and M. Podgòrny, Phys. Rev. B **31**, 7526 (1985).

[32]I.-K. Jeong, F. Mohiuddin-Jacobs, V. Petkov, S. J. L. Billinge, and S. Kycia, Phys. Rev. B **63**, 205202 (2001).

[33]N. Uchitomi, H. Endo, H. Oomae, and Y. Jinbo, Thin Solid Films **519**, 8207 (2011).

[34]H. Ohno, Science **281**, 951 (1998).

[35]L. Chen, S. Yan, P. F. Xu, J. Lu, W. Z. Wang, J. J. Deng, X. Qian, Y. Ji, and J. H. Zhao, Appl. Phys. Lett. **95**, 182505 (2009).

[36]T. Jungwirth, K. Y. Wang, J. Mašek, K. W. Edmonds, J. König, J. Sinova, M. Polini, N. A. Goncharuk, A. H. MacDonald, M. Sawicki, A. W. Rushforth, R. P. Campion, L. X. Zhao, C. T. Foxon, and B. L. Gallagher, Phys. Rev. B **72**, 165204 (2005).

[37]K. Wang, R. Campion, K. Edmonds, M. Sawicki, T. Dietl, C. Foxon, and B. Gallagher, AIP Conf. Proc. **772**, 333 (2005).

[38]N. Uchitomi, H. Inoue, T. Kato, H. Toyota, and H. Uchida, J. Appl. Phys. **117**, 17B905 (2015).